

Absorption Spectra and Electron-Vibration Coupling of Ti:Sapphire From First Principles

Hua Bao¹

Assistant Professor
University of Michigan-Shanghai Jiao Tong
University Joint Institute,
Shanghai Jiao Tong University,
Shanghai 200240, China
e-mail: hua.bao@sjtu.edu.cn

Xiulin Ruan¹

Associate Professor
School of Mechanical Engineering and
Birck Nanotechnology Center,
Purdue University,
West Lafayette, IN 47907
e-mail: ruan@purdue.edu

First-principles calculations are performed to study the absorption spectra and electron-vibration coupling of titanium-doped sapphire (Ti:Al₂O₃). Geometry optimization shows a local structure relaxation after the doping of Ti. Electronic band structure calculation shows that five additional dopant energy bands are observed around the band gap of Al₂O₃, and are attributed to the five localized d orbitals of the Ti dopant. The optical absorption spectra are then predicted by averaging the oscillator strength during a 4 ps first-principles molecular dynamics (MD) trajectory, and the spectra agree well with the experimental results. Electron-vibration coupling is further investigated by studying the response of the ground and excited states to the E_g vibrational mode, for which a configuration coordinate diagram is obtained. Stokes shift effect is observed, which confirms the red shift of emission spectra of Ti:sapphire. This work offers a quantitative understanding of the optical properties and crystal-field theory of Ti-doped sapphire. The first-principles calculation framework developed here can also be followed to predict the optical properties and study the electron-vibration coupling in other doped materials.

[DOI: 10.1115/1.4032177]

Keywords: radiative heat transfer, first principles, absorption spectra, doped material

1 Introduction

Titanium-doped sapphire (Ti:Al₂O₃) is widely used as a tunable laser material [1], for its broad emission spectrum from 650 to 1100 nm. It is also used to produce ultrashort, ultrahigh-intensity pulses with a duration of 20–100 fs. The optical absorption and emission properties of Ti:sapphire are mainly due to the *d*–*d* transitions of the Ti atoms, and the strong electron-vibration coupling leads to the broad emission spectra. Crystal-field theory has been used extensively to study the optical properties [2–4], and many insightful interpretations have been presented, such as the splitting of 3*d* orbitals due to the crystal field, Jahn–Teller effect, and the Stokes shift [2–4]. Quantitative modeling of the absorption and emission properties, however, still rely on parameters fitted from experimental data.

First-principles calculations provide a possibility to quantitatively predict these properties with the initial crystal structure as the only input. Recently, there has been a growing interest in the radiative heat transfer community on the first-principles based method to study the radiative properties of solid materials. Methods based on first principles have been developed to predict optical absorption and/or optical constants of bulk materials (such as GaAs [5] and SiC [6]) as well as nanomaterials (such as quantum dots [7] and carbon nanotubes [8,9]). These predictions could advance our understanding of the detailed material properties in a quantitative manner. The first-principles based calculation also allows us to predict the thermal radiative properties of materials under the conditions when experimental measurements are difficult (for example, high temperature or high pressure). For doped material like titanium-doped sapphire, the optical properties have only been predicted with the “cluster approach,” where it is assumed that the optical properties of Ti:sapphire are completely determined by Ti and the nearest neighboring O atoms. This

approach was applied to a Ti[H₂O]₆³⁺ cluster by Ruan and Kaviani and good results for excited state energy levels were obtained [10]. A small computational capacity is needed for the cluster, but it is not yet justified that the nearest neighbor environment can fully capture the local environment of a doped ion in the host material. Also, the temperature effect is not considered in their calculation [10].

Doped materials are also modeled with a more realistic “supercell approach,” where a relatively large cell of the host material is created, and a dopant is introduced to the supercell. This approach has been performed on doped or defect materials including Cr⁴⁺:YAG [11] and O vacancy defects in sapphire [12], mainly focusing on band structure and defect energy calculation. Ti:sapphire has been investigated using the supercell approach to obtain the formation energy for interstitial and substitutional Ti dopant [13]. All these works have used static ground state calculations to understand structural properties and electron band structure of doped systems. Although electron band structure is related to the optical transitions, the optical absorption and emission process (especially the broadening of absorption and emission peaks) are also strongly dependent on the coupling with vibrational modes. The static ground state calculation cannot capture these effects and is thus not possible to predict the full absorption spectra. Recently, the MD methods have been adopted to allow a time-domain approach to include the effect of lattice vibration. For example, using first-principles MD methods, Bao et al. predicted the temperature-dependent optical absorption of a PbSe nanocrystal [7] and the broadening of absorption peak of GaAs in far infrared spectrum [14]. Yang et al. predicted the high-temperature optical absorption of SiC using a similar approach [15]. However, these methods have not yet been applied to understand the optical properties of an ion-doped dielectric material.

In this work, we present the framework of predicting the optical absorption and electron–phonon coupling in Ti:sapphire by first-principles calculations, treating Ti:sapphire as a periodically doped solid. A 120-atom supercell with a substitutional Ti³⁺ dopant is considered. Impurity structure and electronic energy levels are first investigated. Then, the finite-temperature optical

¹Corresponding authors.

Contributed by the Heat Transfer Division of ASME for publication in the JOURNAL OF HEAT TRANSFER. Manuscript received August 25, 2015; final manuscript received November 30, 2015; published online January 12, 2016. Assoc. Editor: Zhuomin Zhang.

absorption spectra are predicted using a first-principles MD approach. Configuration coordinate diagram is further studied for the E_g mode and the spectral electron–phonon coupling strength is investigated. The obtained results are discussed and compared with previous theoretical and experimental results.

2 Electronic Structure

The first-principles plane-wave pseudopotential method is employed with the generalized gradient approximation (GGA) using Perdew–Wang exchange and correlation functional [16], as implemented in the VASP [17] package. Vanderbilt ultrasoft pseudopotentials [18] are used for Ti and O, while the Rappe–Rabe–Kaxiras–Joannopoulos [19] type norm-conserving pseudopotential is used for Al. Partial core is included in Ti and Al potentials. The choice of pseudopotentials follows Ref. [13]. An electron energy cutoff of 400 eV has been used for all calculations.

Corundum (Al_2O_3) has a rhombohedral cell with 30 atoms and a $R\bar{3}c$ symmetry group. To minimize the dopant–dopant interaction, a large rhombohedral supercell with 120 atoms is constructed from four unit cells. One Al atom is replaced by a Ti atom, creating a substitution-type point defect as shown in Fig. 1. No ambiguity is introduced since all Al ions are equivalent in terms of symmetry. The cell parameters are chosen as $a = 9.5204 \text{ \AA}$ and $c = 12.9933 \text{ \AA}$, following experimental data [20].

The supercell is relaxed with fixed cell size and shape. We do not attempt to relax the cell parameters. Although replacing one Al atom with Ti atom will change the lattice constant in our calculation, this effect is not physical in real Ti:sapphire, in which the Ti dopants atoms are sufficiently dilute and have negligible effect on the lattice constant of the host. Because of the large size of the supercell, only Γ point in the first Brillouin zone is used for electron integration. As shown in Fig. 1, the Ti ion has six neighboring O ions, which exhibit a distorted octahedral configuration. Only two different Ti–O bond lengths are observed, indicating that the Ti–O octahedral complex preserves the symmetry of Al–O complex in the host material. The bond length values of Ti–O are 1.961 and 2.071 \AA , which are larger compared to the Al–O bond lengths 1.856 and 1.971 \AA . The difference can be attributed to the larger ionic radius of Ti ions. The average Ti–O bond length is 2.016 \AA , similar to 2.01 \AA acquired by Matsunaga et al. [13].

The electronic band structure of the supercell is then calculated. Since we are only interested in the electronic and optical properties of the Ti-dopant, only energy levels at the Γ point of the Brillouin zone are shown in Fig. 2. Due to the ionic nature of Ti:sapphire, energy levels can easily be identified. The valence

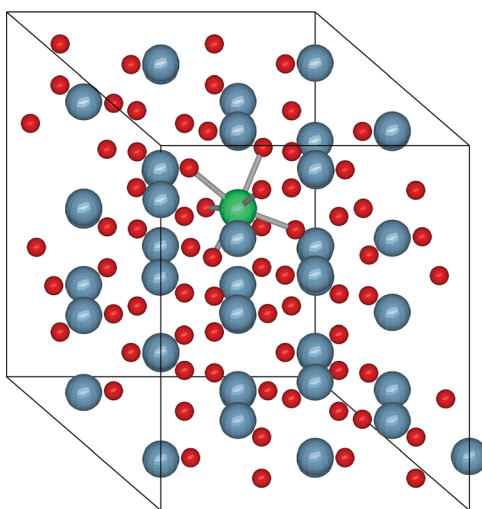


Fig. 1 The optimized structure for a doped 120 ion Ti:Al₂O₃ supercell

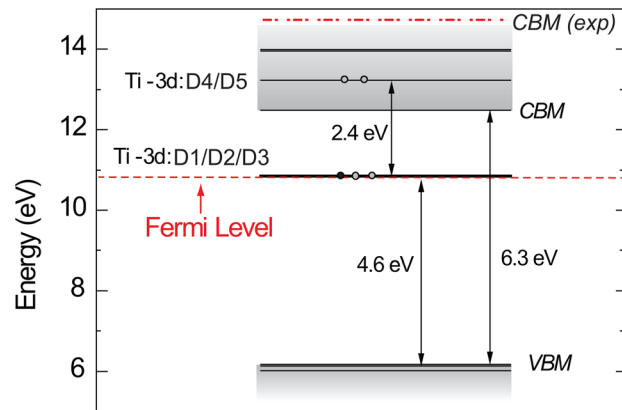


Fig. 2 Electronic energy levels for the Ti-doped alumina supercell. The lower Ti 3d level is three-fold degenerate (D1, D2, and D3 denoted by the three circles) and the upper Ti 3d level is two-fold degenerate (D4 and D5 denoted by the two circles).

band maximum (VBM) is consisted of O 2p orbitals, and the conduction band minimum (CBM) is Al 3s orbitals. The intrinsic band gap value of the supercell is calculated to be 6.3 eV, which is similar to other calculated band gap value of pure alumina (6.4 eV [21,22]). This confirms that our doping concentration is small enough, so that the dopant will not affect the electronic property of the host material. All the calculated values are smaller than the experimental value 8.7 eV [23], which is normal considering GGA calculations tend to underestimate the band gap value [24].

There are five additional energy levels induced by the Ti dopant, denoted from low energy to high energy as D1 to D5. These levels can be identified as Ti 3d orbitals, which split into lower three (T_{2g}) and upper two (E_g) energy levels in the Al₂O₃ host. The three T_{2g} levels are nearly degenerate with small splitting value around 0.01 eV, and E_g levels are also nearly degenerate. The splitting is small so that it is difficult to be observed in Fig. 2. The charge distributions of D1 and D4 orbitals are shown as isosurfaces [25] in Fig. 3. It is clear that the isosurfaces resemble the lobe shapes of typical 3d orbitals and also contain some components of p orbitals of the adjacent O atoms. This confirms that the D1 and D4 energy levels are mainly localized energy states of the Ti dopant. The calculated splitting energy 2.4 eV is consistent with experimental results [2]. The energy of the T_{2g} levels is 4.6 eV above the VBM, which is also in good agreement with a previous prediction of 4.66 eV [13] and with the experimental

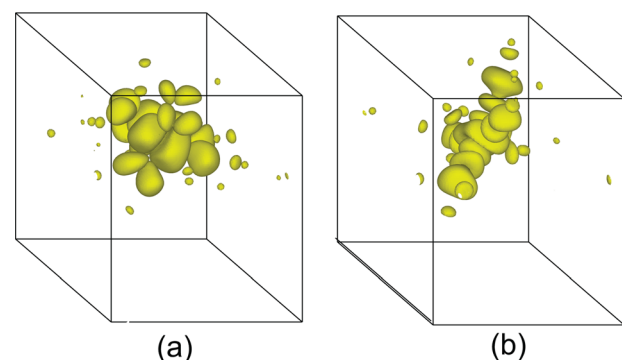


Fig. 3 Charge density isosurfaces where the magnitude of the charge density is $3.4 \times 10^{-10} \text{ e}$ per unit cell. (a) The charge distribution of the D1 orbital. (b) The charge distribution of D4 orbital. It can be seen that these states are highly localized around the Ti dopant. The shape of the lobes around the Ti dopant resembles the typical d orbital.

estimate (4.45 eV) [26]. However, due to the underestimation of the intrinsic band gap, the E_g levels, which are supposed to be located in the intrinsic band gap, are above the CBM. Since the calculation of optical properties will not involve VBM, we do not correct this.

The calculated electronic structure can be compared with the well-known crystal-field theory, which has been the primary theory to explain the formation of impurity levels. According to crystal-field theory, the free Ti^{3+} ion has five degenerate d orbitals. After the ion is placed in an octahedral crystals field, the orbitals will split into one doubly degenerate E_g multiplet (including $d_{x^2-y^2}$ and d_{z^2} orbital) and one triply degenerate T_{2g} multiplet (including d_{xy} , d_{yz} , and d_{zx} orbitals) [2]. Our results are consistent with the crystals field theory in that the five energy levels are split into lower three (D1, D2, and D3) and upper two (D4 and D5) bands. It should be noted that further splitting of the T_{2g} level due to Jahn–Teller effect cannot be captured by the first-principles calculations presented here. To consider this effect, it is necessary to perform excited state calculation for the doped system [10], which is difficult with current computational capacity.

3 Absorption Spectra

The electron transition probability between two energy levels is characterized by the absorption cross section $\sigma_a(\omega)$, given by [27]

$$\sigma_a(\omega) = \frac{\pi e^2}{2\epsilon_0 mc} f_{ij} \quad (1)$$

in which f_{ij} is the oscillator strength between two energy levels; e , m , ϵ_0 , and c are the electron charge, electron mass, vacuum permittivity, and speed of light, respectively. Oscillator strength can be determined by [27]

$$f_{ij} = \frac{2m\omega}{3\hbar e^2} |\langle i|\mathbf{r}|j\rangle|^2 \quad (2)$$

where the $\langle i|$ and $|j\rangle$ are the wave functions of the initial and final state, respectively, and \mathbf{r} is the position vector. In our first-principles calculation of Ti:sapphire, the wave functions are approximated by the independent particle orbitals of Ti atom. Also, the oscillator strength is calculated by our own code used previously to calculate the absorption spectra of quantum dots [7], in which the spatial integral is performed over the supercell. Note that our approach simply follows Eq. (2), which is not the same as the general approach based on the linear response theory [28] for extended system. Different from semiconductors, Ti:sapphire is an ion-doped dielectric and its optical properties are determined primarily by transitions of localized electrons of Ti dopants in the crystal field. In the practical range of doping concentration, the dopants are rather far apart and their localized electrons do not interact. Therefore, its optical properties have little dependence on whether the dopants are arranged periodically, and our approach is valid. Results in Sec. 2 show that the T_{2g} to E_g energy levels in Ti:sapphire form six pairs of such transitions. Thus, the summation of six line transitions should give the absorption spectra of this material. However, lattice vibrations also interfere with the local crystal field at the optically active Ti ion and affect the optical absorption and decay process, which is a typical electron-vibration coupling process. Vibration can modulate the electronic energy levels, leading to broadening and shifting of optical spectra. Lattice vibrations are therefore needed to be included in the system to obtain an absorption spectrum that contains the vibration effect.

In order to consider the broadening of absorption spectra due to the electron-vibration coupling, first-principles MD is then performed for this supercell. The system is first heated to around 300 K using a simple velocity rescale technique. After the temperature becomes stable, a 4 ps microcanonical trajectory (NVE ensemble) is generated and the data are recorded. The lattice vibration induced by the ionic motion will modify the electronic

structure and the wave function. Also, according to the Fermi–Dirac distribution, the single electron on the lowest T_{2g} level will be excited to other T_{2g} levels. Because of the large energy difference between T_{2g} and other energy levels, the distribution function on other energy levels will not be affected by the temperature. Thus, we approximate the frequency-dependent absorption spectra by averaging the six pair transitions at each ionic configuration during the MD process

$$\sigma(\omega) = \frac{C}{N} \sum_n \sum_{ij} \beta_i f_{ij} \delta(\omega - \omega_{ij}) \quad (3)$$

where i denotes an energy level from T_{2g} levels and j is an E_g level; and β_i is the occupation number of level i . N is the total number of MD time steps and C is a constant which can be determined from Eq. (1).

The calculated Ti:sapphire spectra and the experimental absorption and emission spectra are shown in Fig. 4. Since the absorption depends on doping density, the peak height cannot be directly compared with experimental results. As such, we normalized the peak heights to unity to only compare the peak position and the spectra broadening. Our calculation results, especially the vibration-induced broadening, agree well with the experiments. In our results, the spectra are not smooth, which is likely due to the insufficient ensemble average limited by the total MD steps we can perform. The emission spectra are centered at a longer wavelength and different from absorption spectra. This is due to the difference between absorption and emission process: during absorption, one assumes the system is in ground state (i.e., D1/D2/D3 have one electron and D4/D5 are empty) and during emission, the system is at excited state (D4/D5 are occupied). To accurately predict emissions process needs excited states calculation. To capture the red shift (Stokes shift) of the emission spectra, we construct the configuration coordinate diagram for the Ti:sapphire, as discussed below.

4 Configuration Coordinate Diagram

The absorption and emission of Ti:sapphire depend on d – d transitions of the Ti^{3+} ion. Since this transition involves a change in crystal-field configuration, the transition energy is very sensitive to the strength of the crystal field. In order to understand how local vibration can affect the electron transition, we construct the configuration coordinate diagram to describe the transition between electronic energy levels coupled to local lattice vibrations. It is a one-dimensional diagram that gives the electronic

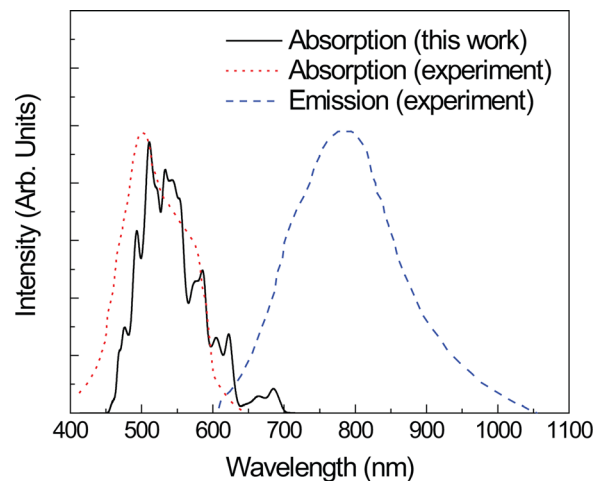


Fig. 4 Calculated absorption spectra at 300 K in this work (black solid line) and the experimental absorption spectra at room temperature [29] (dotted line) and emission spectra from Ref. [30] (dashed line)

energy levels with respect to the ion displacement along a certain normal vibrational mode. Because Ti dopant ion differs in mass and charge from Al ions, local modes are used that have different frequencies from the host lattice. From Fig. 3, we know that the energy levels mainly involve the d orbitals of Ti dopant and p orbitals of the six neighboring O ions. Thus, the relative positions of the nearest O ions have the most important effect on the crystal field on the dopant. Based on these considerations, we assume that the lattice vibrational effects are attributed to the vibrational modes of the octahedral complex (with Ti in the center and six O ion around). The local vibrational modes are shown in Fig. 5, and the modes are characterized by its symmetry (A_{1g} , E_g , T_{1g} , T_{1u} , and T_{2u}) [2,10]. The configuration coordinate diagram of E_g vibrational mode is obtained by manually displacing the six O atoms along a pattern with E_g symmetry with a scaling factor Q , and the diagram is shown in Fig. 6. The lowest curve is the total ground state energy with respect to the normal coordinate, and the upper curves are the energy levels which represent the higher state.

Based on the adiabatic approximation, the electronic transitions are instantaneous compared to the ion motion and are thus represented by vertical lines in the diagram, as shown in Fig. 6. The most probable absorption transition takes place at the minimum of the ground state, with an excitation energy of 2.4 eV, as shown in the absorption spectra. The most probable radiative decay takes place from the two minimums of the E_g level, corresponding to transition energies of around 2.2 eV. The two energies are corresponding to the two R-lines at the high-energy edge in the low-

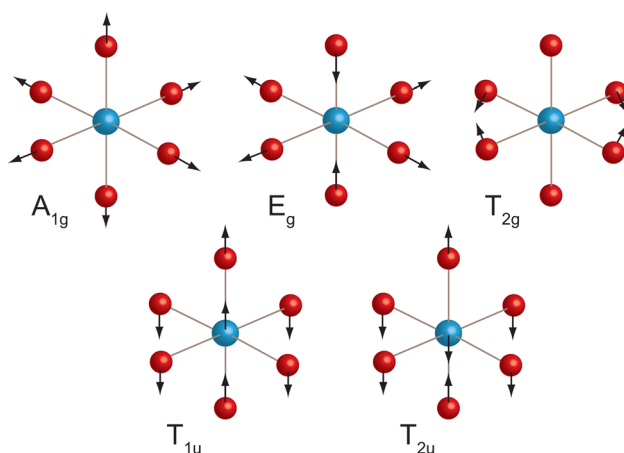


Fig. 5 The five different local vibrational modes of Ti octahedra

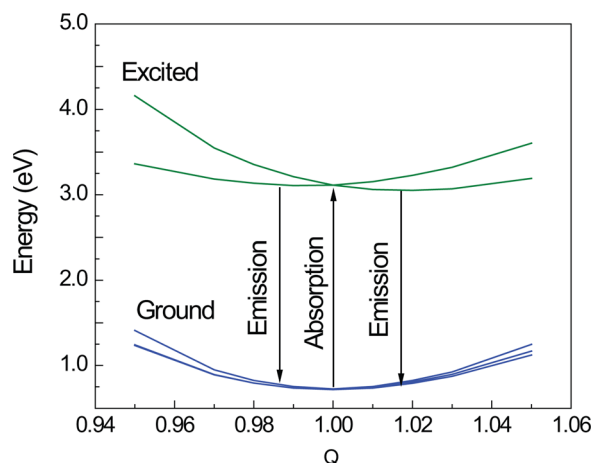


Fig. 6 Configuration coordinate diagram for E_g vibrational mode

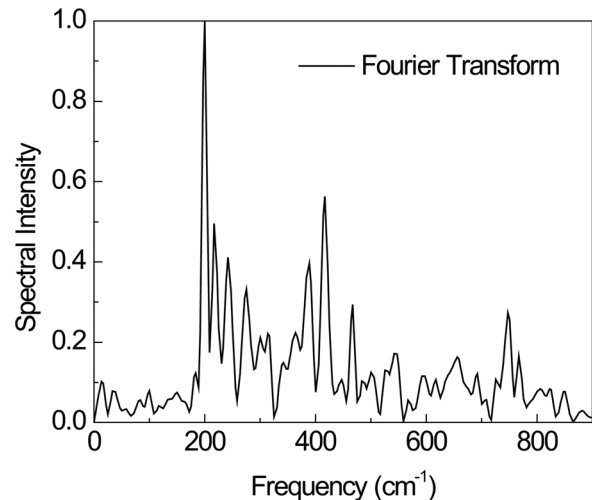


Fig. 7 Fourier transform of transition energy during a 4 ps trajectory

temperature fluorescence spectra of Ti:sapphire, but the values are a little higher, due to the fact that the high-energy level is taken as the excited state energy. The shift of the energy (or wavelength) between absorption spectra and emission spectra is the well-known Stokes shift. Though the Stokes shift is captured here, it is smaller than the experimental results, which show that the absorption spectra and emission spectra are centered at around 500 and 750 nm (2.48 and 1.65 eV), respectively [2].

5 Electron-Vibration Coupling Spectra

The coupling of electrons and vibration is directly related to the second derivative of the energy along the nuclear trajectory, and therefore, those vibrational modes that most strongly modulate the energy levels create the largest coupling [31]. To analyze the electron-vibration coupling strength, the Fourier transform of the transition energy is calculated and shown in Fig. 7. Here, the transition energy is defined as the energy difference between the average energy of T_{2g} levels and the average of E_g levels. The spectral intensity shows that the phonons that most strongly couple to this transition energy are concentrated between 200 and 450 cm^{-1} . This frequency corresponds to the E_g and A_{1g} vibrational modes of the Ti–O complex, which are calculated to be 379 and 429 cm^{-1} , respectively [10]. Frequencies of other three eigenmodes are all below 200 cm^{-1} (T_{2g} , T_{1u} , T_{2u}). This result agrees well with the prediction of theory that E_g mode plays the most important role in the vibronic coupling of Ti:sapphire.

6 Summary and Discussion

In summary, we have used first-principles pseudopotential calculations to obtain the electronic structure and configuration coordinate diagram of Ti:sapphire. When Al ions are replaced by Ti ions, the O ions relax to allow for a 5% longer Ti–O bond than the Al–O bond. Five extra energy levels appear around the band gap. These levels split into lower three and higher two degenerate groups, separated by 2.4 eV. These energy levels are mainly composed of Ti 3d orbital and p orbitals of the six nearest neighbor O atoms, and are strongly localized at the Ti sites. The absorption spectra are then predicted by a MD approach, and the result agrees well with the experimental results. We also quantitatively constructed the configuration coordinate diagram for E_g mode of the Ti octahedra and observed Stokes shift. The predicted Stokes shift value, however, is smaller compared to the experimental result. This is because the current ground state calculation uses independent particle approximation, where the excited states are approximated by the higher energy level. Accurate prediction of the

Stokes shift requires more advanced method beyond the density functional theory we used here, such as time-dependent density functional theory and excited states dynamics, which only recently have become feasible on solid state systems [32,33]. This could be left for further investigation.

Acknowledgment

This work was partly supported by a faculty startup fund from Purdue University. H.B. acknowledges the support by the National Natural Science Foundation of China (Grant No. 51306111) and Shanghai Municipal Natural Science Foundation (Grant No. 13ZR1456000).

Nomenclature

a = lattice constant
 c = lattice constant, speed of light
 e = elementary charge
 f = oscillator strength
 \hbar = reduced Planck's constant
 i, j = wave function label
 m = mass
 N = total number of MD steps
 Q = scaling factor
 \mathbf{r} = position vector
 β = occupation number
 ϵ_0 = dielectric permittivity of vacuum
 σ_a = absorption cross section
 ω = angular frequency

References

- [1] Moulton, P., 1982, "Ti-Doped Sapphire Tunable Solid-State Laser," *Opt. News*, **8**(6), p. 9.
- [2] Powell, R., 1998, *Physics of Solid-State Laser Materials*, Springer-Verlag, New York.
- [3] Kikoin, K., and Fleurov, V., 1994, *Transition Metal Impurities in Semiconductors*, World Scientific Publishing, Singapore.
- [4] Grinberg, M., and Mandelis, A., 1994, "Photopyroelectric-Quantum-Yield Spectroscopy and Quantum-Mechanical Photoexcitation-Decay Kinetics of the Ti^{3+} Ion in Al_2O_3 ," *Phys. Rev. B*, **49**(18), pp. 12496–12506.
- [5] Bao, H., and Ruan, X. L., 2010, "Ab Initio Calculations of Thermal Radiative Properties: The Semiconductor GaAs," *Int. J. Heat Mass Transfer*, **53**(7–8), pp. 1308–1312.
- [6] Yang, J., Liu, L., and Tan, J., 2014, "First-Principles Molecular Dynamics Study on Temperature-Dependent Dielectric Function of Bulk 3C and 6H SiC in the Energy Range 3–8 eV," *Physica B*, **436**, pp. 182–187.
- [7] Bao, H., Habenicht, B. F., Prezhdo, O. V., and Ruan, X. L., 2009, "Temperature Dependence of Hot Carrier Relaxation in a PbSe Nanocrystal: An Ab Initio Study," *Phys. Rev. B*, **79**(23), p. 235306.
- [8] Sisto, A., Ruan, X., and Fisher, T. S., 2014, "First Principles and Finite Element Predictions of Radiative Properties of Nanostructure Arrays: Single-Walled Carbon Nanotube Arrays," *ASME J. Heat Transfer*, **136**(6), p. 062702.
- [9] Yang, J., Liu, L., and Tan, J., 2015, "First-Principles Study on Dielectric Function of Isolated and Bundled Carbon Nanotubes," *J. Quant. Spectrosc. Radiat. Transfer*, **158**, pp. 78–83.
- [10] Ruan, X. L., and Kaviani, M., 2008, "Ab Initio Calculations of the Photon-Electron-Phonon Interactions in Laser Cooling of Ion-Doped Solids," *J. Comput. Theor. Nanosci.*, **5**, pp. 221–229.
- [11] Ching, W., Xu, Y.-N., and Briceen, B., 1999, "Ab-Initio Calculation of Excited State Absorption of Cr^{4+} in $\text{Y}_3\text{Al}_5\text{O}_{12}$," *Appl. Phys. Lett.*, **74**(25), pp. 3755–3757.
- [12] Xu, Y.-N., Gu, Z.-Q., Zhong, X.-F., and Ching, W. Y., 1997, "Ab Initio Calculations for the Neutral and Charged Vacancy in Sapphire," *Phys. Rev. B*, **56**(12), pp. 7277–7284.
- [13] Matsunaga, K., Nakamura, A., Yamamoto, T., and Ikuhara, Y., 2003, "First-Principles Study of Defect Energetics in Titanium-Doped Alumina," *Phys. Rev. B*, **68**(21), p. 214102.
- [14] Bao, H., Qiu, B., Zhang, Y., and Ruan, X. L., 2012, "A First-Principles Molecular Dynamics Approach for Predicting Optical Phonon Lifetimes and Far-Infrared Reflectance of Polar Materials," *J. Quant. Spectrosc. Radiat. Transfer*, **113**(13), pp. 1683–1688.
- [15] Yang, J. Y., Liu, L. H., and Tan, J. Y., 2014, "Temperature-Dependent Dielectric Function of Germanium in the UV-vis Spectral Range: A First-Principles Study," *J. Quant. Spectrosc. Radiat. Transfer*, **141**, pp. 24–31.
- [16] Perdew, J. P., and Zunger, A., 1981, "Self-Interaction Correction to Density-Functional Approximations for Many-Electron Systems," *Phys. Rev. B*, **23**, pp. 5048–5079.
- [17] Kresse, G., and Furthmüller, J., 1996, "Efficiency of Ab-Initio Total Energy Calculations for Metals and Semiconductors Using a Plane-Wave Basis Set," *Comput. Mater. Sci.*, **6**(1), pp. 15–50.
- [18] Vanderbilt, D., 1990, "Soft Self-Consistent Pseudopotentials in a Generalized Eigenvalue Formalism," *Phys. Rev. B*, **41**, pp. 7892–7895.
- [19] Rappe, A. M., Rabe, K. M., Kaxiras, E., and Joannopoulos, J. D., 1990, "Optimized Pseudopotentials," *Phys. Rev. B*, **41**(2), pp. 1227–1230.
- [20] Lewis, J., Schwarzenbach, D., and Flack, H., 1982, "Electric Field Gradients and Charge Density in Corundum, $\alpha\text{-Al}_2\text{O}_3$," *Acta Cryst.*, **A38**, pp. 733–739.
- [21] Matsunaga, K., Yamamoto, T., and Ikuhara, Y., 2003, "First-Principles Calculations of Intrinsic Defects in Al_2O_3 ," *Phys. Rev. B*, **68**(8), p. 085110.
- [22] Ching, W., and Xu, Y.-N., 1994, "First-Principles Calculation of Electronic, Optical, and Structural Properties of $\alpha\text{-Al}_2\text{O}_3$," *J. Am. Ceram. Soc.*, **77**(2), pp. 404–411.
- [23] Bortz, M., and French, R., 1989, "Optical Reflectivity Measurements Using a Laser Plasma Light Source," *Appl. Phys. Lett.*, **55**(19), pp. 1955–1957.
- [24] Pulci, O., Onida, G., Sole, R. D., and Reining, L., 1998, "Ab Initio Calculation of Self-Energy Effects on Optical Properties of GaAs(110)," *Phys. Rev. Lett.*, **81**(24), pp. 5374–5377.
- [25] Momma, K., and Izumi, F., 2006, "An Integrated Three-Dimensional Visualization System Vesta Using wxWidgets," *Commission Crystallogr. Comput., IUCr Newslett.*, No. 7, pp. 106–119.
- [26] Mohapatra, S., and Kröger, F., 1977, "Defect Structure of $\alpha\text{-Al}_2\text{O}_3$ Doped With Titanium," *J. Am. Ceram. Soc.*, **60**(9–10), pp. 381–387.
- [27] Hilborn, R., 1982, "Einstein Coefficients, Cross Sections, f Values, Dipole Moments, and All That," *Am. J. Phys.*, **50**(11), pp. 982–986.
- [28] Gonze, X., 1997, "First-Principles Responses of Solids to Atomic Displacements and Homogeneous Electric Fields: Implementation of a Conjugate-Gradient Algorithm," *Phys. Rev. B*, **55**(16), pp. 10337–10354.
- [29] Aggarwal, R. L., Sanchez, A., Fahey, R. E., and Strauss, A. J., 1986, "Magnetic and Optical Measurements on $\text{Ti:Al}_2\text{O}_3$ Crystals for Laser Applications: Concentration and Absorption Cross Section of Ti^{3+} Ions," *Appl. Phys. Lett.*, **48**(20), pp. 1345–1347.
- [30] Rapoport, W. R., and Khattak, C. P., 1988, "Titanium Sapphire Laser Characteristics," *Appl. Opt.*, **27**(13), pp. 2677–2684.
- [31] Kilina, S. V., Craig, C. F., Kilin, D. S., and Prezhdo, O. V., 2007, "Ab Initio Time-Domain Study of Phonon-Assisted Relaxation of Charge Carriers in PbSe Quantum Dot," *J. Phys. Chem. C*, **111**(12), pp. 4871–4878.
- [32] Bernasconi, L., Tomić, S., Ferrero, M., Réart, M., Orlando, R., Dovesi, R., and Harrison, N. M., 2011, "First-Principles Optical Response of Semiconductors and Oxide Materials," *Phys. Rev. B*, **83**(19), p. 195325.
- [33] Bernasconi, L., 2015, "Chaotic Soliton Dynamics in Photoexcited Trans-Polyacetylene," *J. Phys. Chem. Lett.*, **6**(5), pp. 908–912.